Impact of ground-motion duration on nonlinear structural performance: Part II: site- and building-specific analysis

Kenneth Otárola, M.EERI[1] ⓘD**, Luis Sousa, M.EERI[2],
Roberto Gentile, M.EERI[3]** ⓘD**, and Carmine
Galasso, M.EERI[1,4]**

Abstract

This study's Part I proved that ground-motion duration could play an important role when assessing the nonlinear structural performance of case-study inelastic single degree-of-freedom systems. However, quantifying duration effects in many practical/more realistic engineering applications is not trivial, given the difficulties in decoupling duration from other ground-motion characteristics. This study's Part II, introduced in this article, explores the impact of duration on nonlinear structural performance by numerically simulating the structural response of realistic case-study reinforced concrete bare and infilled building frames. Advanced computational models incorporating structural components' cyclic and in-cycle strength and stiffness deterioration, and destabilizing $P - \Delta$ effects are used. The proposed methodology relies on the generalized conditional intensity measure approach to select ground motions. This allows selecting records consistent with the seismic hazard at a target site, both in terms of spectral shape and duration. Those are employed as input to cloud-based nonlinear structural response analyses. Variance analysis is used to quantify the impact of duration on structural response. Furthermore, vector-valued fragility and vulnerability models alternatively using peak- and cumulative-based engineering demand parameters are derived. Results show that higher damage/loss estimates can be attained as ground-motion duration increases. Relative differences up to 44% are found in fragility median values for a *pre-code* reinforced concrete infilled frame when comparing scalar and vector-valued fragility models conditioned on average pseudo-spectral acceleration and significant durations up to 35 s.

[1]Department of Science, Technology and Society, Scuola Universitaria Superiore IUSS Pavia, Pavia, Italy
[2]Verisk—Extreme Event Solutions, London, UK
[3]Institute for Risk and Disaster Reduction, University College London, London, UK
[4]Department of Civil, Environmental and Geomatic Engineering, University College London, London, UK

Corresponding author:
Carmine Galasso, Department of Civil, Environmental and Geomatic Engineering, University College London, Bloomsbury Campus, Gower Street, London WC1E 6BT, UK.
Email: c.galasso@ucl.ac.uk

Introduction

This study's Part I (i.e. Otárola et al., 2023) presented a comprehensive parametric analysis to quantitatively evaluate the impact of ground-motion duration on the nonlinear structural performance of case-study inelastic single degree-of-freedom systems using spectrally equivalent long- and short-duration ground motions in comparative incremental dynamic analyses. Overall, it provided the required tools to assess the impact of ground-motion duration in large-scale (regional) seismic risk assessment exercises, as per current practice (e.g. Martins and Silva, 2021; Villar-Vega et al., 2017). This study's Part II, described in this article, proposes an end-to-end seismic performance-based assessment framework to account for spectral shape and duration effects in more practical/realistic engineering applications, such as single-building loss assessments. Specifically, it considers a site-specific seismic hazard analysis based on the generalized conditional intensity measure (GCIM) approach (Bradley, 2010) and a structure-specific seismic response modeling based on cloud analyses (e.g. Jalayer and Cornell, 2009) of multi-degree-of-freedom (MDoF) systems. The considered systems represent realistic reinforced concrete (RC) bare and infilled building frames associated with different seismic design levels. In addition, this study uses peak- and cumulative-based engineering demand parameters (EDPs) and a vector of intensity measures (IMs) accounting for ground-motion spectral shape and duration.

It is known that ground-motion duration increases with the distance from the source due to the scattering and dispersion of seismic waves and the difference in the arrival times of waves propagating at different velocities and crossing different paths (e.g. Boore and Thompson, 2014; Stein and Wysession, 2003; Trifunac and Brady, 1978). However, duration also depends on local site conditions, with long-duration ground motions typically observed at sites with soft soils due to repeated seismic wave reflections within the softer layers (e.g. Dobry et al., 1978). Hence, ground-motion record selection for seismic performance-based assessment should adequately consider the site-specific seismic hazard, accounting for the various sources of uncertainty associated with such hazard estimates. An inaccurate record selection might lead to biased results in terms of structural response and resulting damage/loss estimates (e.g. Sousa et al., 2017). This selection typically involves searching within a ground-motion database to find records related to specific seismological and site features (e.g. rupture mechanism, earthquake magnitude, source-to-site distance, soil type) and ground-motion amplitude, frequency content, and—more rarely—duration consistent with the seismic hazard at the considered site.

The definition of target distributions of ground-motion IMs for a given site and a rational approach to match these targets are fundamental for a rigorous site-specific, hazard-consistent ground-motion record selection (Bradley, 2010). The conditional spectrum (CS) approach developed by Baker and Cornell (2006) and improved by Jayaram et al. (2011) offers a direct link between ground-motion characteristics and probabilistic seismic hazard analysis (PSHA), providing the mean and variance of pseudo-spectral acceleration (*SA*) ordinates conditioned on the occurrence of a specific value of *SA* at the

fundamental structural period ($SA(T_1)$; commonly known as conditioning intensity level) for a given scenario or intensity level (i.e. mean return period), eventually determined through PSHA. With the GCIM approach, Bradley (2010) extended the CS concept to any vector of ground-motion IMs, establishing that for a given earthquake rupture within the source model used in PSHA, this conditional vector-valued IM also has a multivariate lognormal distribution. This concept enables ground-motion record selection conditioning on a variety of IMs, allowing simultaneously considering ground-motion amplitude, frequency content, and duration characteristics.

Chandramohan et al. (2016a) used the GCIM approach to computing site-specific target distribution of ground-motion IMs (including and excluding a duration-related IM) to assemble ground-motion record sets for three sites located in different tectonic settings (characterized by shallow-crustal and subduction earthquake events). Thereby, the effects of considering duration when estimating the structural collapse risk of a ductile RC building frame were quantified by performing multiple-stripe analyses for the different record sets, representing the structural response in terms of maximum (i.e. peak) inter-story drift ratio (MIDR). Neglecting duration led to underestimating the mean annual frequency of collapse for every considered study case, in particular, up to 59.00% for a site where subduction earthquake events dominate the seismic hazard. Previously, Chandramohan et al. (2016b) observed that it is unlikely to detect any influence of ground-motion duration on the structural response at low conditioning intensity levels because duration effects are apparent after the structural components reach their peak strength and start to strain-soften. Thus, duration impact on structural response can be more evident at sites presenting high-intensity, long-duration ground motions.

Du et al. (2020) investigated duration effects on structural collapse risk using hazard-consistent ground-motion record sets selected based on the GCIM approach, similarly to Chandramohan et al. (2016a). However, this study quantitatively investigated duration effects using several scenarios with varying earthquake magnitude, source-to-site distance, and conditioning fundamental structural periods. For each scenario, four hazard-consistent ground-motion record sets with a different distribution of ground-motion IMs were selected (in particular, one base-duration set and three longer-duration sets). Fragility relationships associated with structural collapse were derived by conducting incremental dynamic analyses on four different steel building frames, representing the structural response in terms of MIDR. Comparative results demonstrated that an impact due to duration could be observed depending on the ratio between the mean significant duration of two (longer/base) sets, having statistically significant effects for ratios over 1.40. In addition, reductions in fragility median values up to 20.00% were obtained using the longer-duration sets compared to the base-duration one. Such reductions are smaller than those obtained in other studies because records from shallow-crustal (rather than subduction) earthquake events were employed (e.g. Bravo-Haro and Elghazouli, 2018; Chandramohan et al., 2016a).

The problems encountered when selecting hazard-consistent ground-motion records for assessing the impact of ground-motion duration on a building (or group of buildings) non-linear structural performance at a specific site are complicated by the observed correlations between duration and other ground-motion characteristics (e.g. spectral shape) influencing structural response (e.g. Bradley, 2011; Huang and Galasso, 2019; Huang et al., 2020). In Part I of this study and specific literature (e.g. Chandramohan et al., 2016b), spectrally equivalent long- and short-duration ground motions were used, assuming a low correlation between spectral shape and duration. Nevertheless, this assumption is not always valid,

especially at sites where multiple sources influence the site-specific seismic hazard. Hence, this study presents an approach to evaluate the specific impact of duration by decoupling it from the effect of other relevant ground-motion characteristics. To this aim, an analysis of variance (ANOVA) approach is employed to analyze the statistical significance of duration effects on structural response. In addition, vector-valued fragility and vulnerability models depending on spectral shape and duration are derived to account for duration influence in more realistic/practical engineering applications like those related to seismic performance-based assessment.

Several nonlinear dynamic analysis procedures that use a vector of IMs to estimate the probabilistic relationship between ground-motion intensity and structural response have been developed (e.g. Baker, 2007). Options include cloud-based analysis, incremental dynamic analysis, and multiple-stripe analysis. Cloud-based analysis, which uses multiple linear regression (commonly through the least-squares approach) on the vector of IMs, requires the fewest number of nonlinear dynamic analyses and can effectively avoid the "curse of dimensionality" issue (Page and Bellman, 1962) (noting that collinearity between IMs can be a problem). In this study, this analysis procedure is implemented to develop vector-valued fragility and vulnerability models using: (a) nonlinear modeling strategies accounting for cyclic and in-cycle strength and stiffness deterioration in structural components and destabilizing $P - \Delta$ effects; (b) EDPs that allow accounting for duration either implicitly (e.g. using advanced hysteretic deterioration models together with peak-based EDPs) or explicitly (e.g. using advanced hysteretic deterioration models together with cumulative-based EDPs); and (c) highly efficient and sufficient (Luco and Cornell, 2007) IMs able of capturing both the effects of ground-motion spectral shape and duration.
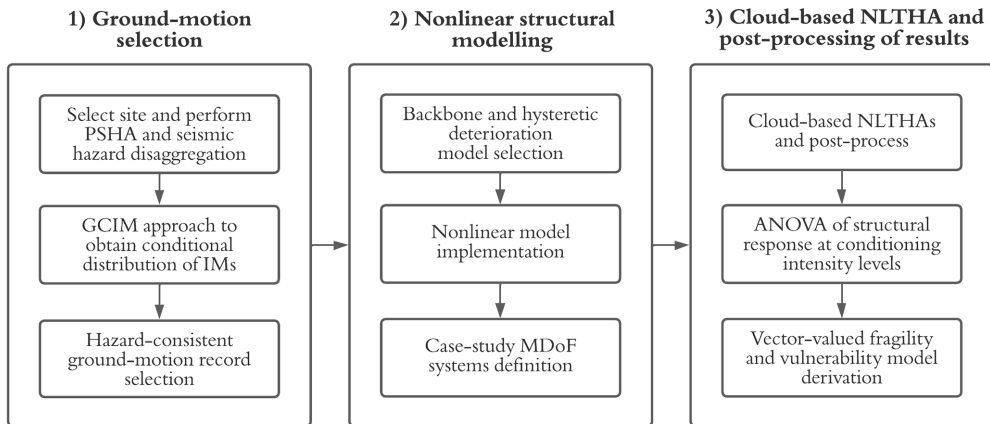
Indeed, Part I of this study (among others) demonstrated that peak-based EDPs did not show a clear correlation with ground-motion duration unless advanced nonlinear modeling strategies (accounting for cyclic and in-cycle strength and stiffness deterioration) were used. However, duration effects on several structural systems were generally observed at conditioning intensity levels producing significant inelastic deformations (especially when approaching their peak strength and beginning to strain-soften as in Chandramohan et al., 2016b), which in turn causes a reduction in the strength, particularly evident in highly deteriorating systems. Conversely, cumulative-based EDPs (e.g. dissipated hysteretic energy, E_h) showed a much stronger correlation since, by definition, they increase monotonically with the duration of the seismic excitation. Therefore, both MIDR and E_h are used in this study to represent the structural response and investigate duration influence on nonlinear structural performance of case-study structures. In such manner, based on the main findings/methods presented in Part I and the results herein introduced, the novelties of this study can be summarized as follows:

- Accounting for ground-motion duration and spectral shape: the GCIM approach is used to select ground-motion records accounting for their duration and spectral shape (accounting for several *SA* ordinates), differently from other studies that only account for ground-motion duration and *SA* at the fundamental structural period ($SA(T_1)$; e.g. Chandramohan et al., 2016a). This approach is deemed more appropriate for site-specific, hazard-consistent analysis. It is worth noting that the selected target site is influenced by multiple sources that, in turn, affect the seismic hazard (e.g. Iervolino et al., 2010). Notably, this study adopts structural systems with low fundamental structural periods, investigating their response at intensity levels associated with a wide variety of seismic hazard return periods. Therefore, a correlation

between ground-motion duration and spectral amplitudes (at different structural periods) is expected (e.g. Huang et al., 2020; Iervolino et al., 2011).

- Vector-valued IM composed of spectral shape and duration: a vector-valued IM consisting of average pseudo-spectral acceleration (*avgSA*) and 5%–95% significant duration (Ds_{5-95}) (i.e. [*avgSA*, Ds_{5-95}]) is used, given the inability to decouple ground-motion duration from the spectral shape at a specific site. To the authors' knowledge, this is the first application of vector-valued IMs to account for ground-motion duration and spectral shape in nonlinear structural performance. This differs from other studies that exclusively used scalar IMs (e.g. Belejo et al., 2017; Pan et al., 2020, among others). Using such a vector-valued IM allows one to adequately capture and reduce the record-to-record and site-to-site variability in the structural response and, consequently, in the damage and loss estimates. This also removes the need to derive fragility and vulnerability models for long- and short-duration ground motions separately, as in previous studies (e.g. Belejo et al., 2017; Bravo-Haro and Elghazouli, 2018; Chandramohan et al., 2016b; Pan et al., 2020).

- Adoption of contributing masonry infills on RC building frames: two different archetypical RC moment-resisting frames representing actual buildings are chosen for analysis. Each building is associated with a different seismic design level, sharing the same geometrical layout. Moreover, two planar building computational models are built for each archetypical building frame (including stiffness and strength in-cycle and cyclic deterioration, and $P - \Delta$ effects), one model in an infilled and the other in a bare configuration (i.e. a total of four study cases). To the authors' knowledge, the impact of ground-motion duration on RC-infilled building frames' nonlinear structural performance has not been studied in previous literature. This study evaluates ground-motion duration effects on bare and infilled building frames under the same settings (i.e. including or excluding masonry infills' contribution to the global strength and stiffness of a corresponding archetypical frame).

- Implementation of E_h as EDP to quantify structural response: a harmonized approach to include E_h in seismic performance-based assessment practice is introduced, including a model to estimate energy-based damage state (DS) thresholds for the case-study structures. Previous studies relied exclusively on damage indices (e.g. Barbosa et al., 2017) to implicitly account for E_h or used peak-based EDPs when using deterioration models that depend on E_h (e.g. Bravo-Haro and Elghazouli, 2018). The approach proposed here differs significantly and includes the adverse effects of directly having several inelastic cycles during long-duration seismic excitations, capturing better the structural behavior from yielding to collapse. The impact of ground-motion duration on structural response is evaluated via ANOVA. To the authors' knowledge, this is the first application of such an approach in this context, differing from the typical hypothesis testing in many other studies (e.g. Iervolino et al., 2006).

This article is organized as follows. Section "Methodology" describes the methodology employed in this study, namely the ground-motion selection procedure and the approach to assess the impact of ground-motion duration on the nonlinear structural performance. Section "Results and discussion" presents the main findings from the analyses based on thoroughly examining the results. These results are also compared against relevant literature findings mentioned before. Section "Conclusions" outlines the main conclusions from the results of this study.

1) **Ground-motion**
selection

2) **Nonlinear structural**
modelling

3) **Cloud-based NLTHA and**
post-processing of results

Select site and perform PSHA and seismic hazard disaggregation	Backbone and hysteretic deterioration model selection	Cloud-based NLTHAs and post-process
GCIM approach to obtain conditional distribution of IMs	Nonlinear model implementation	ANOVA of structural response at conditioning intensity levels
Hazard-consistent ground-motion record selection	Case-study MDoF systems definition	Vector-valued fragility and vulnerability model derivation

Figure 1. Adopted methodology to assess the impact of earthquake-induced ground-motion duration on nonlinear structural performance.
PSHA: probabilistic seismic hazard analysis; GCIM: generalized conditional intensity measure; IM: intensity measure (amplitude- and duration-related IMs); MDoF: multi-degree-of-freedom; ANOVA: analysis of variance; NLTHA: nonlinear time-history analysis.

Methodology

The adopted methodology (Figure 1) relies on the GCIM approach to select site-specific, hazard-consistent ground-motion records for a target site affected by multiple seismic sources. Those records are used as input to perform cloud-based analyses on case-study RC building frames representing the selected target site. The impact of ground-motion duration on nonlinear structural performance is then investigated via ANOVA, and vector-valued fragility and vulnerability models corresponding to each structure. Details related to each aspect of this methodology are introduced in the specific subsections.

Case-study structural systems

Two distinct archetypical infilled RC moment-resisting frames representing buildings located in Ponticelli—Napoli, Italy—are selected (latitude: 40.8516°, longitude: 14.3446°). Each building is associated with a different seismic design level, constituting the mid-rise RC building vulnerability class used in this study. Nevertheless, both frames share the same geometry (Minas and Galasso, 2019), with a total height equal to 13.50 m, a first story height equal to 4.50 m and upper stories of 3.00 m, and bay spans of 4.50 m (Figure 2a). Furthermore, two planar building computational models are developed for each archetypical building frame, one in an infilled and the other in a bare configuration for relative comparison (i.e. to evaluate ground-motion duration effects on bare and infilled building frames under the same settings); hence, a total of four study cases (Figure 2b). These models are intended to capture the three-dimensional structural behavior representing the geometry, boundary conditions, mass distribution, energy dissipation, and interaction among structural components based on the assumption that the buildings are regular and symmetric. In other words, the models can simulate the structural response of the buildings in both horizontal directions equivalently under an earthquake event (i.e. ground motion) (e.g. Haselton and Deierlein, 2008).
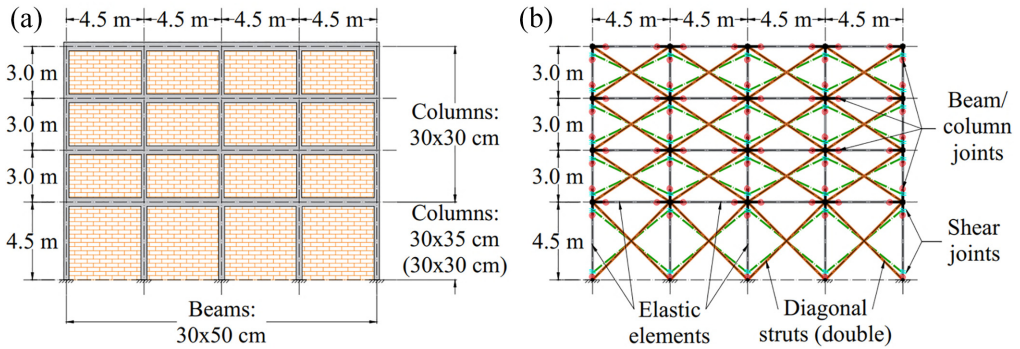
Figure 2. (a) Elevation layout of the PI and PB frames; (b) nonlinear modeling strategy for the PI and PB frames. Equivalent diagonal struts do not apply to the PB frame.

The first building frame, termed *special-code* frame, is designed and detailed according to the Eurocode 8 Part 3 (EC8-3) seismic provisions for high ductility class (EN 1998-3, 2005). These provisions include capacity design, various requirements in terms of cross-sectional dimensions, and seismic detailing to ensure ductile global performance and prevent the formation of localized brittle failure mechanisms. It is characterized by 30×50 cm^2 columns at the first level, 30×40 cm^2 columns at the second and third levels, 30×30 cm^2 columns at the fourth level, and 30×50 cm^2 beams. The other building frame, termed *pre-code* frame, is designed only for gravity loads according to the Royal Decree n. 2239 of 1939 (Consiglio dei Ministri, 1939) that regulated the structural design in Italy until 1974. Thus, the frame does not conform to modern seismic requirements and is characterized by a non-ductile behavior due to the lack of capacity design principles, poor confinement, and susceptibility to developing brittle failure mechanisms. It is characterized by 30×30 cm^2 columns at all levels except for the internal 30×35 cm^2 columns at the first level, and 30×50 cm^2 beams. According to the above denomination, the four case-study frames are identified as *special-code* infilled (SI) frame, *pre-code* infilled (PI) frame, *special-code* bare (SB) frame, and *pre-code* bare (PB) frame, based on their level of seismic design and structural configuration.

The materials' mean mechanical properties, such as the concrete's compressive strength and the steel rebar yield strength, represent those adopted in Italy (Table 1). Specifically, the mean mechanical properties of the concrete are obtained from the Verderame et al. (2011) investigations for the PI and PB frames while being based on current practice of building construction for the SI and SB frames (Aljawhari et al., 2021). The mean mechanical properties of the masonry infills are obtained from Liberatore and Mollaioli (2015) for the PI frame, while they are obtained from Mohammad Noh et al. (2017) for the SI frame (Table 2). It is worth mentioning that the masonry infills for bare frames function as heavy partitions and do not contribute to the overall strength or stiffness of the structural systems but undoubtedly contribute to losses. In addition, some basic information on the case-study frames' dynamic structural behavior, such as the fundamental structural periods and the corresponding mass participation ratios, is summarized in Table 3.

Numerical modeling strategy

The case-study frames' structural response is simulated using two-dimensional computational models in OpenSees v3.2.2 (Mazzoni et al., 2009). The gravity loads are uniformly

Table 1. Properties of the RC

Parameter	Symbol	Units	PI/PB frame	SI/SB frame
Compressive strength of the concrete	f_{cm}	MPa	19.00	37.00
Modulus of elasticity of the concrete	E_c	GPa	26.67	32.60
Yield strength of the steel rebars	f_{ym}	MPa	360.00	490.00
Modulus of elasticity of the steel rebars	E_s	GPa	200.00	200.00

PI: *pre-code* infilled; PB: *pre-code* bare; SI: *special-code* infilled; SB: *special-code* bare.

Table 2. Properties of the masonry infills

Parameter	Symbol	Units	PI frame	SI frame
Compressive strength	σ_{m0}	MPa	2.20	4.20
Shear strength	τ_{m0}	MPa	0.44	0.33
Vertical gravity stress	σ_0	MPa	0.00	0.00
Sliding resistance	τ_0	MPa	0.39	0.23
Modulus of elasticity	E_m	GPa	2.40	2.31
Thickness of infills	t_m	cm	14.50	10.00

PI: *pre-code* infilled; SI: *special-code* infilled.

Table 3. Fundamental structural periods and mass participation ratios

Parameter	PI frame	PB frame	SI frame	SB frame
Fundamental structural period	$T_1 = 0.27$ s $T_2 = 0.08$ s	$T_1 = 0.80$ s $T_2 = 0.24$ s	$T_1 = 0.20$ s $T_2 = 0.06$ s	$T_1 = 0.50$ s $T_2 = 0.16$ s
Mass participation ratio	98.06%	94.50%	97.53%	91.96%

PI: *pre-code* infilled; PB: *pre-code* bare; SI: *special-code* infilled; SB: *special-code* bare.

distributed on the beams, and the masses are concentrated at each floor master node (associated with the assigned rigid diaphragms in each story). Elastic damping is modeled through the Rayleigh model (Zareian and Medina, 2010) using a 5.00% viscous damping ratio on the first two structural vibration modes. Geometric nonlinearities are incorporated to account for the destabilizing $P - \Delta$ effects due to the gravity loads. Beam-column end-offsets and floor diaphragms are both modeled as rigid components.

A lumped plasticity approach is used for all the case-study frames to model both beams and columns' nonlinear behavior using zero-length rotational springs. The Ibarra–Medina–Krawinkler (Ibarra et al., 2005; Lignos and Krawinkler, 2011) model with a peak-oriented hysteretic response is implemented to define the moment–rotation relationship of the rotational springs (including stiffness and strength cyclic and in-cycle deterioration). The yielding bending moment and yielding rotation are determined according to Panagiotakos and Fardis (2001), while the other parameters (i.e. initial stiffness, hardening stiffness, maximum bending moment, rotation at the onset of capping, softening stiffness, and post-capping rotation) are defined according to Haselton et al. (2016) (including axial

effects in the constitutive models). The former study is based on the results of 1000 tests, mainly cyclic, for different RC structural components, while the latter provides formulations based on cyclic and monotonic tests of 255 RC columns failing in flexural or flexural-shear modes. For PI and PB frames, nonlinear shear springs are added in series to the rotational ones to account for potential shear failures that may occur in such frames. This is attributed to the lack of transverse reinforcement and smooth bars with end-hooks, especially in external joints (e.g. Calvi et al., 2002a, 2002b; Pampanin et al., 2002). In fact, the shear failure mode is unlikely to develop in modern frames since those were designed with actual seismic design provisions. The Setzler and Sezena (2008) model (including axial gravity load effects in the constitutive models) is implemented to define the force–deformation relationship of the shear springs following a peak-oriented hysteretic behavior. It is characterized by the maximum shear strength (calculated according to Sezen and Moehle, 2004), shear deformation at the onset of peak shear strength, the shear deformation at the beginning of shear failure, and the shear deformation at the axial load failure. Masonry infill walls are modeled as equivalent diagonal struts connecting beam–column intersections to account for their effect on the global response of the case-study frames. The force–deformation relationship introduced by Liberatore and Decanini (2011) is assigned to the equivalent struts characterizing the behavior of infills, which accounts for four possible failure modes: diagonal tension, sliding shear, corner crushing, and diagonal compression, following a peak-oriented hysteretic behavior with pinching and suffering from cyclic stiffness and in-cycle strength deterioration. The parameters describing the hysteretic response of infills are adopted from Mohammad Noh et al. (2017), who calibrated them based on experimental testing, characterized by the uncracked infill stiffness, the strength at the first crack, the displacement at the first crack, the stiffness at complete cracking, the maximum strength, the full crack displacement, the residual strength, and the residual displacement. Diagonal struts which connect the nodes at the beam–column intersections are used to model the masonry infills for the SI frame. In contrast, infills are modeled using Burton and Deierleins' (2014) double strut approach for the PI frame. In such a case, one diagonal strut connecting the beam–column joints and another off-diagonal strut connecting the column shear springs are modeled. According to Burton and Deierlein (2014), 75% of total infill strength and stiffness is assigned to the diagonal strut, while 25% is assigned to the off-diagonal one. Such a strategy does not simulate the entire distribution of column shear due to the frame–infill interaction. Still, it captures the increase in shear demands in columns, thus allowing possible changes in the overall plastic mechanism of the frame. A complete description and additional details (e.g. structural parameters descriptions) of the used models can be found in Aljawhari et al. (2021).

Ground-motion record selection

The Ds_{5-95}, as defined in Part I of this study, is considered an efficient and sufficient IM (e.g. Chandramohan et al., 2016b). It describes the time interval within a ground-motion record related to the strongest shaking, influenced by the earthquake-induced body and surface waves (e.g. Kempton and Stewart, 2006). There are several advantages when using Ds_{5-95} to represent ground-motion duration, such as (a) it is expressed in time units; (b) it is unaffected by ground-motion amplitude scaling; (c) it is well correlated to cumulative-based EDPs; and (d) it is hazard-computable as various ground-motion models (GMMs) have been proposed in the literature for such IM (e.g. Douglas, 2021).

Since ground-motion records represent the critical link between PSHA results and seismic structural response, the explicit consideration of the joint probability distribution of

spectral shape and duration is required to achieve an accurate result. The selection procedure used in this study is based on the GCIM approach (Bradley, 2010). The conditional distributions of amplitude- and duration-based IMs are computed using seismic hazard disaggregation results, GMMs, and empirical correlation models between the total residuals of the chosen IMs. The ground-motion records used herein are obtained from the Pacific Earthquake Engineering Research Center – Next Generation Attenuation Relationships for Western United States database (NGA-West2; Ancheta et al., 2014), dominated by shallow-crustal earthquake events as in Part I. It is worth noting again that duration effects are found to be significant at ratios between the mean significant duration of long- and short-duration ground-motion sets as low as 1.40 (e.g. Du et al., 2020); therefore, a noticeable impact due to duration on the nonlinear structural performance is expected in such seismicity conditions. The GMMs and empirical correlation models calibrated from Italian strong-motion records for amplitude- and integral-based IMs are used in this study (Huang and Galasso, 2019; Huang et al., 2020).

As mentioned before, a target site (i.e. Ponticelli) influenced by multiple sources, each contributing to the site-specific seismic hazard, is selected (e.g. Barani et al., 2009). Such a condition can reflect the existing correlation between spectral amplitudes (at different structural periods) and duration. Notably, this study adopts structural systems with a low fundamental structural period (i.e. the correlation between spectral shape and duration is expected; e.g. Huang et al., 2020), investigating their structural response at intensity levels associated with a wide variety of seismic hazard return periods. Hence, seismic hazard disaggregation showing a bimodal distribution of earthquake magnitudes and source-to-site distances contributing to ground-motion exceedance are not expected for the structural periods of interest (e.g. Iervolino et al., 2010, 2011). The target site is located over class C soil (Forte et al., 2019) according to EC8, with a mean shear wave velocity in the first 30 m (Vs_{30}) of 331 m/s. The source model adopted for the analysis is the one depicted in Barani et al. (2009), after modifying the maximum probable magnitude in "zone 927" from 7.30 to 7.00 since the adopted GMM and empirical correlation models are reliable up to this value. This assumption does not represent a significant drawback since Italy's maximum registered earthquake had a moment magnitude equal to 6.90.

PSHA and seismic hazard disaggregation are computed using the OpenQuake engine (Silva et al., 2014). Seismic hazard disaggregation is performed following a rupture-by-rupture discretization (i.e. accounting for all the independent ruptures generated by the earthquake rupture forecast), as proposed by Sousa et al. (2017). The vector of IMs considered in this work includes Ds_{5-95}, peak-ground acceleration, and 35 distinct SA ordinates within a range of fundamental structural periods from 0.10 up to 4.00 s. Using the GCIM approach, 17 sets of hazard-consistent ground-motion records are selected for various conditioning $SA(T_1)$ levels within a range of values from 0.05 up to 2.00 g for all the case-study frames. It is worth mentioning that a 2500-year return period $SA(T_1)$ level equal to 1.14 g is attained for the target site (based on the PSHA results).

The algorithm used for ground-motion record selection is proposed by Bradley (2012), where random realizations (i.e. simulations) of the selected IMs (consistent with the GCIM target distributions) are generated. Therefore, for each realization of a vector of IMs, a ground motion with an identical IM vector can be ideally selected. In this study, the algorithm is slightly modified to admit a maximum amplitude scale factor of 5.00 (Luco and Bazzurro, 2007) and avoid repeated utilization of the same seed ground-motion records within each specific conditioning intensity level. As an example, Figure 3a shows the response spectra of the selected ground-motion records and the Ds_{5-95} distributions for a
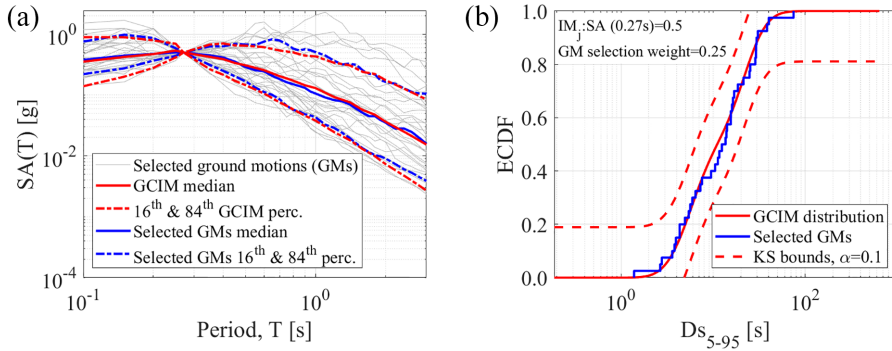
Figure 3. GCIM distributions and selected ground motions for the PI frame: (a) ground-motion response spectra; (b) empirical cumulative distribution function (ECDF) of the selected ground motions and Kolmogorov–Smirnov (KS) testing for Ds_{5-95}.

conditioning $SA(T_1) = 0.50\ g$ for the PI frame. Since higher-mode effects are not likely to dominate the structural behavior (Table 3), mismatches between the GCIM realizations and the selected ground-motion SA ordinates below the fundamental structural period are not considered a major issue.

The selection is repeated for each case-study frame and each conditioning intensity level. The 40 ground-motion records within the database with the minimum misfit compared to the target GCIM distributions are selected for each conditioning intensity level. This is done using the Kolmogorov–Smirnov goodness-of-fit testing for each of the 37 IM distributions, as shown in Figure 3b. The main parameters used in the selection are as follows: (a) weight's vector, equal to 0.25 for Ds_{5-95} and 0.75/36 for other IMs; (b) significance value (α) for the KS test bounds, equal to 0.10; and (c) the number of random realization replicates, equal to 10. More related details on the considered record selection strategy can be found in Bradley (2012).

Seismic response analysis

For each case-study frame, a nonlinear time-history analysis (NLTHA) is conducted for each selected ground motion at each $SA(T_1)$ conditioning intensity level. Provided that the analysis outcomes are represented using $SA(T_1)$, this would result in multiple stripes (typically in a multiple-stripe analysis). However, the geometric mean of the pseudo-spectral accelerations in a range of periods (i.e., *avgSA*) is herein selected to represent the response, thus resulting in a cloud of points in the EDP versus IM space. This IM selection allows having a good proxy of both amplitude and spectral shape (Eads et al., 2015; Kohrangi et al., 2017) while ensuring efficiency and sufficiency. *avgSA* is calculated using the following SA ordinates: $0.2T_1$; $\min[1.5T_2, (T_1 + T_2)/2]$; T_1; $1.5T_1$; $2.0T_1$ (Kazantzi and Vamvatsikos, 2015). Figure 4a to d illustrates the results of the seismic response analysis, both expressed using a peak-based EDP (i.e. MIDR) and a cumulative-based one (i.e. E_h) for the PI frame. As expected, nonlinear structural responses increase as *avgSA* and Ds_{5-95} increase. Moreover, as suggested in Part I, the response is better correlated to E_h than MIDR, with a Pearson correlation coefficient (ρ) (in log–log space) equal to 0.31 and 0.14, respectively. It is worth noting that a CS-based ground-motion record selection using *avgSA* has been proposed by Kohrangi et al. (2017). However, this approach is not used in the present study as ground-motion duration is not explicitly considered in the record
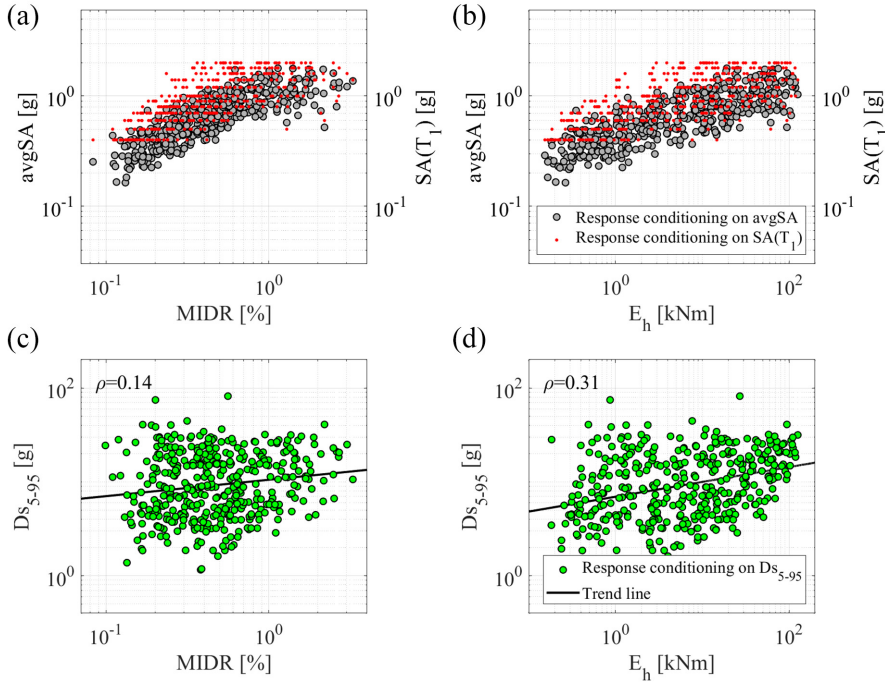
Figure 4. Response analysis of the PI frame expressed in terms of (a) MIDR, conditioning on *avgSA* or $SA(T_1)$; (b) E_h, conditioning on *avgSA* or $SA(T_1)$; (c) MIDR, conditioning on Ds_{5-95}; (d) E_h, conditioning on Ds_{5-95}. Structural responses at conditioning intensity levels providing (fully) elastic cases (near-zero E_h values) and collapse cases are not included.

selection approach proposed by Kohrangi et al. (2017), as opposed to the GCIM-based ground-motion record selection of Bradley (2012).

DS thresholds definition

Structure-specific DS thresholds in terms of MIDR are calibrated via pushover analyses reviewing multiple measurable criteria according to Table 4. The pushover load pattern is defined according to the first-mode shape, as indicated in EC8-3 (EN 1998-3, 2005). Figure 5a and b shows the first story MIDR versus base-shear coefficient capacity curves for the case-study frames. In every case, the definition of the DS thresholds is governed by the MIDR response associated with this story (i.e. the first floor). The selected DS thresholds are shown in Table 5; as expected, the SI and SB frames have significantly higher thresholds concerning the PI and PB frames. Structural collapse (dynamic instability not associated with a numerical value of the EDPs) is defined in this study as reaching an MIDR of 4.00% for the PI and PB frames and 8.00% for SI and SB frames. Such collapse DS thresholds are indifferently used (i.e. when using MIDR or E_h as EDP) to produce the collapse fragility models.

Energy-based DS thresholds are defined using the stable relationship between MIDR and E_h (e.g. Gentile and Galasso, 2021; Quinde et al., 2021), as also explained in this study's Part I. To do so, the structural response data (Figure 6a; distribution of Ds_{5-95} and obtained structural response) are used to fit the median MIDR versus E_h relationship in the exponential
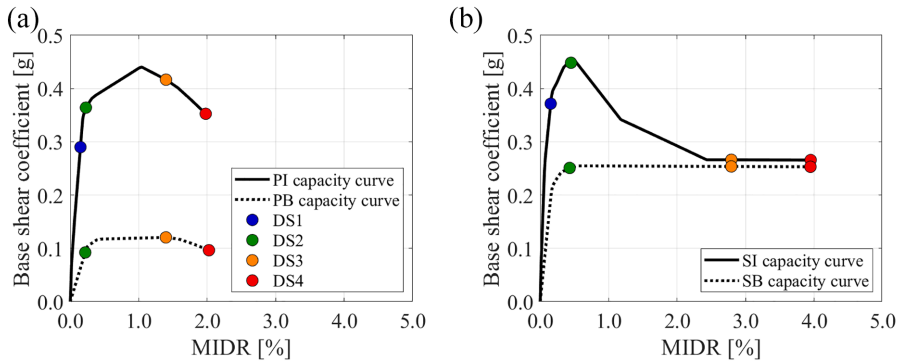
Figure 5. (a) Capacity curve for the PI and PB frame and (b) capacity curve for the SI and SB frame. The colored circles correspond to the DS threshold definition (Table 4).

Table 4. Criteria used to define the DS thresholds of the case-study frames (Aljawhari et al., 2021)

Damage level	Slight damage (DS1)	Moderate damage (DS2)	Extensive damage (DS3)	Complete damage (DS4)
Section level	N/A	Reaching yield bending strength in a supporting column.	Reaching maximum bending strength in any column.	Reaching shear failure in any of the structural components.
Component level	First masonry infill panel starts to develop cracks.	Reaching yield rotation in a supporting column.	Reaching 75% ultimate rotation in any component.	Reaching ultimate rotation in any component.
Global level	N/A	Reaching global yield strength of the structure.	Reaching global maximum strength of the structure.	Reaching 20% drop in global maximum strength of the structure.
DSs description	Non-structural damage only due to masonry infill cracking.	Moderate structural and non-structural damage with no significant yielding of structural components.	Severe structural and non-structural damage. Some residual strength and stiffness are retained.	Full exploitation of strength and ductility. Very low residual strength and stiffness in the components.

DS: damage state.

Table 5. Definition of DS thresholds in terms of MIDR (DS1 does not apply to PB and SB frame)

Case study	DS1	DS2	DS3	DS4
PI/PB frame	0.16%	0.25%	1.40%	2.00%
SI/SB frame	0.15%	0.45%	2.80%	4.00%

DS: damage state; MIDR: maximum inter-story drift ratio; PB: *pre-code* bare; SB: *special-code* bare; PI: *pre-code* infilled; SI: *special-code* infilled.
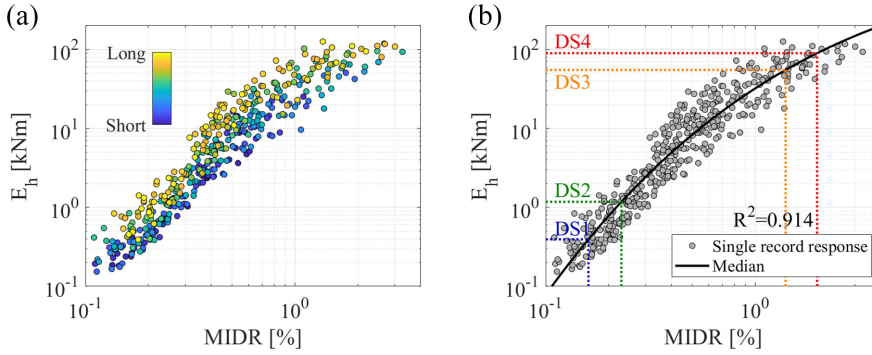
Figure 6. Definition of energy-based DS thresholds from the MIDR versus E_h relationship for the PI frame: (a) Ds_{5-95} distribution for the structural response associated with each selected ground-motion record; (b) energy-based DS thresholds definition. Structural responses at conditioning intensity levels providing (fully) elastic cases (near-zero E_h values) and collapse cases are not included.

form in Equation 1 and shown in Figure 6b. Such a relationship is fitted by least-squares non-linear regression in log–log space. In this equation, a_0, a_1, a_2, and a_3 are the coefficients of the regression. It is worth mentioning that structural responses at conditioning intensity levels providing (fully) elastic cases (near-zero E_h values) and collapse cases (not associated with a numerical value of the EDPs as stated above) are omitted:

$$E_h(MIDR) = \exp(a_0 MIDR^{a_1} + a_2 MIDR^{a_3}) \qquad (1)$$

Such functional form allows, from a statistical (rather than physics-based) perspective, capturing the change in the concavity of the MIDR versus E_h relationship, which tends to be positive if—for a given value of the MIDR—the backbone tangent stiffness of the structure is positive, and vice versa (Gentile and Galasso, 2021). Equation 1 is used to convert the deformation-based DS thresholds into energy-based ones, thus allowing one to retain the adopted DS thresholds' reliability while obtaining cumulative-based thresholds in median terms, which are deemed more appropriate for a study involving ground-motion duration. Nevertheless, relevant experimental/field data may be used to provide a deeper confirmation of such a hypothesis. A more extensive discussion about the peak deformation versus energy relationship can be found in Part I of this study. It is worth recalling that consistently with the common practice of neglecting the variability of the MIDR-based DS thresholds in deriving fragility relationships, the MIDR to E_h conversion herein is carried out neglecting the E_h|MIDR variability; therefore, E_h-based DS thresholds are obtained in median terms.

Decoupling duration from spectral shape

To visualize how duration changes with spectral shape and whether the spectral shape effects can be effectively decoupled from duration effects at the selected site, 100 synthetic spectral shapes (i.e. response spectra) and their corresponding Ds_{5-95} are simulated using the GCIM approach. Conditioning periods of 0.50, 1.00, 1.50, and 2.00 s at $SA(T_1)$ levels of 0.20, 0.50, and 0.80 g are considered (12 scenarios in total). The simulations are shown in Figure 7a for $SA(0.50\ s) = 0.50$ g and in Figure 7b for $SA(2.00\ s) = 0.50$ g, as an
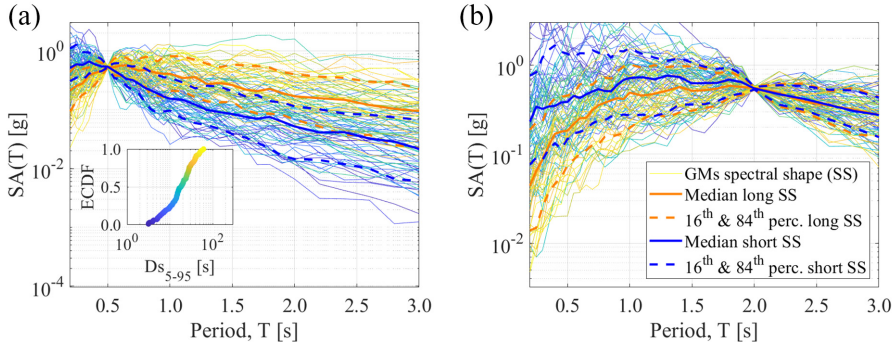
Figure 7. (a) Synthetic spectral shapes and Ds_{5-95} distribution for $SA(0.50\ s) = 0.50\ g$; (b) synthetic spectral shapes for $SA(2.00\ s) = 0.50\ g$ (Ds_{5-95} distribution not shown for brevity). The percentile blue lines are associated with the 50 spectral shapes with the shortest Ds_{5-95}, while percentile yellow lines are associated with the 50 spectral shapes with the longest Ds_{5-95}.

example. It is worth mentioning that those figures refer to $SA(T_1) = 0.50\ g$ only, but the trends are consistent across the considered conditioning intensity levels.

The 50 response spectra with the shortest and the longest Ds_{5-95} are sorted into two groups (arbitrarily named as short and long, respectively). The corresponding median, 16th, and 84th response spectra are estimated for each group. If spectral shape can be effectively decoupled from duration, the above short- and long-response spectra should match, indicating that duration is not correlated to spectral shape (i.e. any duration value can be attained for similar spectral shapes). Figure 7a shows that the percentile response spectra do not match, while the percentile spectra in Figure 7b only match after the fundamental conditioning structural period. If higher-mode effects do not dominate the structural response of the (longer period) systems under consideration, the observed relationships between spectral shape and duration below the fundamental structural period should not affect the results. More in general, as noted herein and according to Huang et al. (2020) (among others; e.g. Bradley, 2011), there is a clear correlation between spectral shape and duration (in the range of −0.55 to 0.10) for conditioning periods up to 1.50–2.00 s (i.e. long fundamental structural periods).

This exercise shows that decoupling duration and spectral shape for the given target site and case-study frames is not possible since the periods of the selected study cases are smaller than 0.83 s (Table 3). In other words, it may not be reasonable to expect two distinct ground motions showing similar spectral shapes yet distinct durations and vice versa. Thus, the approach used in Part I of this study, involving pairs of spectrally equivalent long- and short-duration records, may not be feasible for this site-specific, hazard-consistent analysis.

To overcome the above difficulty, the ANOVA (Fisher, 1992) is adopted to measure the impact of ground-motion duration on nonlinear structural performance. The ANOVA allows measuring the proportion of the total variance in the response (dependent) variable prediction, explained by each predictor (independent) variable. This analysis estimates the contribution of all ground-motion characteristics of interest to the variability in the structural response. Therefore, a comparison between the impact of duration against that of spectral shape is possible. The ANOVA is performed for each conditioning intensity level,

consistently with the GCIM results, using a multiple linear regression through the ordinary least-squares approach, including (a) *avgSA*; (b) Ds_{5-95} and *avgSA*. Equation 2 describes the linear model to estimate the EDPs at each conditioning $SA(T_1)$ level in log–log space. In such equation, IM_i is the *ith* IM out of *n*, b_0 and b_i are the respective regressor coefficients, and ε is a normal random variable with zero mean and standard deviation σ related to the error of the residuals. The proportion of the variance explained measures the impact of ground-motion duration on this linear model; the summation of these values is the so-called coefficient of determination (R^2). The response variables selected for ANOVA are alternatively MIDR and E_h, as mentioned above. It is worth noting that, for this case, the variance is equal to the mean squared error of the regression model; therefore, the standard deviation is equal to the associated root mean squared error:

$$ln(EDP) = b_0 + \sum_{i=1}^{n} b_i ln(IM_i) + \varepsilon \sim N(0, \sigma^2) \tag{2}$$

Vector-valued fragility and vulnerability models

Vector-valued IMs use two or more parameters to predict a structure's response with higher efficiency (Baker and Cornell, 2005) than scalar IMs and attain sufficiency when scalar IMs do not guarantee it (Elefante et al., 2010). In this study, a vector $\boldsymbol{IM} = [avgSA, \ Ds_{5-95}]$ is used to derive fragility and vulnerability models. First, the structural response data are partitioned into two parts: collapse and non-collapse data. It is worth noting that structural responses at conditioning intensity levels providing (fully) elastic cases (near-zero E_h values) are not included in the analysis. A multiple linear regression via the least-squares approach (in log–log space) is used to model the probabilistic seismic demand model representing the EDP median ($\mu_{EDP|\boldsymbol{IM}}$) trend of non-collapsing data (Equation 3) (noting that $ln(\mu_{EDP|\boldsymbol{IM}})$ equals the EDP mean in log–log space since the EDP responses are assumed to follow a lognormal distribution). In such an equation, c_0, c_1, and c_2 are the obtained constant regression coefficients. The logarithmic standard deviation of the proposed model ($\sigma_{ln(EDP)|\boldsymbol{IM}}$) is calculated as the root mean squared error of the residuals. In Figure 8a and b, an example of the models for the PI frame, alternatively considering MIDR and E_h as an EDP is illustrated. As expected, the proportion of the variability explained (i.e. R^2) by the model is higher when using E_h. The collinearity issue between IMs is dismissed through Belsley collinearity diagnostics (Belsley, 1991) for each case-study frame.

$$\mu_{EDP|\boldsymbol{IM}} = c_0 Ds_{5-95}{}^{c_1} avgSA^{c_2} \tag{3}$$

The probability of exceeding a DS conditioned on $\boldsymbol{IM}$ given no collapse (i.e. without including collapse cases), $P(EDP > edp_{DSi}|\boldsymbol{IM}, NC)$, can be estimated as shown in Equation 4. edp_{DSi} stands for the *ith* DS threshold expressed as an EDP. *NC* stands for no collapse:

$$P(EDP > edp_{DSi}|\boldsymbol{IM}, NC) = 1 - \Phi \left[\frac{ln(edp_{DSi}) - ln\left(\mu_{EDP|\boldsymbol{IM}}\right)}{\sigma_{ln(EDP)|\boldsymbol{IM}}} \right] \tag{4}$$

Using the DS thresholds (i.e. edp_{DSi}) and inverting Equation 3, the median ($\mu_{avgSA|DSi, Ds_{5-95}}$) of a given fragility relationship conditioning on the *ith* DS and a specific
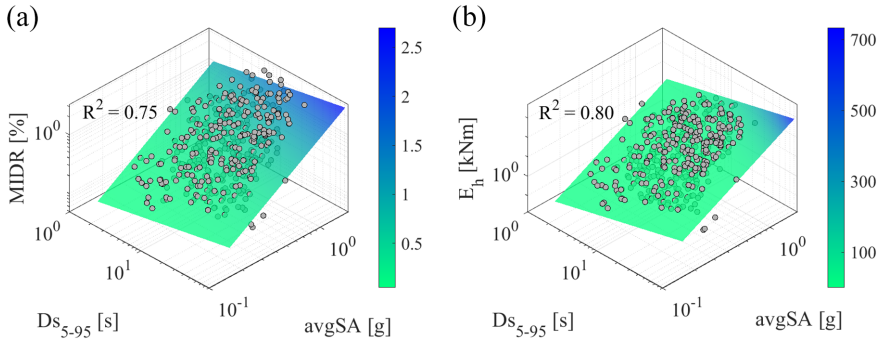
Figure 8. Probabilistic seismic demand model for the PI frame in terms of (a) MIDR; (b) E_h. Structural responses at conditioning intensity levels providing (fully) elastic cases (near-zero E_h values) and collapse cases are not included:

Ds_{5-95} value can be calculated (Equation 5) assuming the data lognormality. Equation 6 provides the associated dispersion ($\beta_{ln(avgSA)\,|\,DSi,\,Ds_{5-95}}$) of the fragility relationship, starting from the logarithmic standard deviation obtained from the developed probabilistic seismic demand models:

$$\mu_{avgSA\,|\,DSi,\,Ds_{5-95}} = \left(\frac{edp_{DSi}}{c_0 Ds_{5-95}{}^{c_1}} \right)^{\frac{1}{c_2}} \tag{5}$$

$$\beta_{ln(avgSA)\,|\,DSi,\,Ds_{5-95}} = \frac{\sigma_{ln(EDP)|\boldsymbol{IM}}}{c_2} \tag{6}$$

Multiple logistic regression (Bojórquez et al., 2012) is used to estimate the probability of collapse, $P(C|\boldsymbol{IM})$, conditioned on $\boldsymbol{IM}$ as shown in Equation 7. In this equation, d_0, d_1, and d_2 are the coefficients to be estimated from this regression. If a single-record structural response caused a collapse, a value equal to one is assigned, and zero otherwise in the context of multiple logistic regression (classification based on a binary approach); C stands for collapse:

$$P(C|\boldsymbol{IM}) = \frac{1}{1 + e^{-[d_0 + d_1 ln(Ds_{5-95}) + d_2 ln(avgSA)]}} \tag{7}$$

The estimated collapse and non-collapse probabilities are then combined using the total probability theorem. Equation 8 is used to compute the conditional probability of exceeding a DS conditioned on $\boldsymbol{IM}$ (e.g. Baker and Cornell, 2005). It is worth repeating that EDP in Equations 3–8 is interchangeable between MIDR and E_h, as appropriate:

$$P(EDP > edp_{DSi}|\boldsymbol{IM}) = P(C|\boldsymbol{IM}) + [1 - P(C|\boldsymbol{IM})]P(EDP > edp_{DSi}|\boldsymbol{IM}, NC) \tag{8}$$

Damage-to-loss ratios (DLRs) are commonly estimated empirically through post-earthquake reconnaissance or employing expert judgment. However, these ratios are region-specific and building class-specific, and they must be carefully selected while developing vulnerability models for obtaining reliable outcomes (e.g. Rossetto and Elnashai, 2003). Since this study involves Italian buildings, a modified version of the DLRs

Table 6. DLRs for the case-study frames

Di Pasquale et al. (2005)	DSs	ND	DS1	DS2	DS3	DS4	DS5
	DLRs	0.00	0.01	0.10	0.35	0.75	1.00
This study	DSs	ND	DS1	DS2	DS3		DS4
	DLRs	0.00	0.01	0.10	0.55		1.00

DS: damage state; DLRs: damage-to-loss ratios; ND: no damage.

suggested by Di Pasquale et al. (2005) is used. The definition of the DLRs for the case-study frames is presented in Table 6. It is worth mentioning that the selected DLRs are representative of all the case studies considered here, according to Aljawhari et al. (2021).

Vector-valued vulnerability models are expressed in terms of mean loss ratio (LR); in other words, the repair-to-replacement cost ratio of the building, conditional on the vector $IM = [avgSA, \ Ds_{5-95}]$ defined earlier. According to Equations 9 and 10, such models are also derived using the total probability theorem. DLR_i is the damage-to-loss ratio (defined deterministically or probabilistically) for the ith DS (i.e. the level of damage), while $P(DS = ds_i|IM)$ is the probability that the DS is equal to ds_i (i.e. the probability of being in a DS) given IM. It is worth noting that the $P(DS = ds_4|IM)$ is equal to $P(DS \geqslant ds_4|IM)$; hence, Equation 10 applies for the other DSs except DS4:

$$LR(IM) = \sum_{i=1}^{4} DLR_i P(DS = ds_i|IM) \tag{9}$$

$$P(DS = ds_i|IM) = P(DS \geqslant ds_i|IM) - P(DS \geqslant ds_{i+1}|IM) \tag{10}$$

Results and discussion

Impact of duration on structural response

An ANOVA is performed for each conditioning intensity level considered within the GCIM approach and each case-study frame. In Figure 9a to d, the proportion of the variance explained for regression models conditioned on $avgSA$ and $[avgSA, \ Ds_{5-95}]$ is illustrated for the PI and SI frames, respectively (the results are consistent among all the case-study frames, other outcomes are not shown for brevity). It is worth mentioning that for low levels of the conditioning $SA(T_1)$, implying elastic response, the structural response shows a particularly low record-to-record variability (confirming that the case studies are first-mode dominated). At such levels, the ANOVA test fails to effectively predict the variability in the structural response, as confirmed via the hypothesis test on the statistical significance of the regressor coefficients (e.g. Kass et al., 1974), with p-values above the typical threshold of 0.05 (i.e. choosing an I-type risk, equal to 0.05) for a 95% of significance, in both $avgSA$ and Ds_{5-95} (i.e. the independent variables of the regression models). Therefore, the ANOVA for the indicated intensity levels (i.e. below $SA(T_1) = 0.30$ and 0.37 g for the PI and SI frames, respectively) is neglected in the subsequent discussion.

Overall, ground-motion duration impacts structural response based on the differences observed between the estimated curves conditioning on $avgSA$ or $[avgSA, Ds_{5-95}]$, and its proportion of explained variance depends on the adopted EDP. It is shown that Ds_{5-95} is better correlated with cumulative-based EDPs, as evidenced by the increased proportion of variance explained by this IM when using E_h, as also observed in Barbosa et al. (2017)
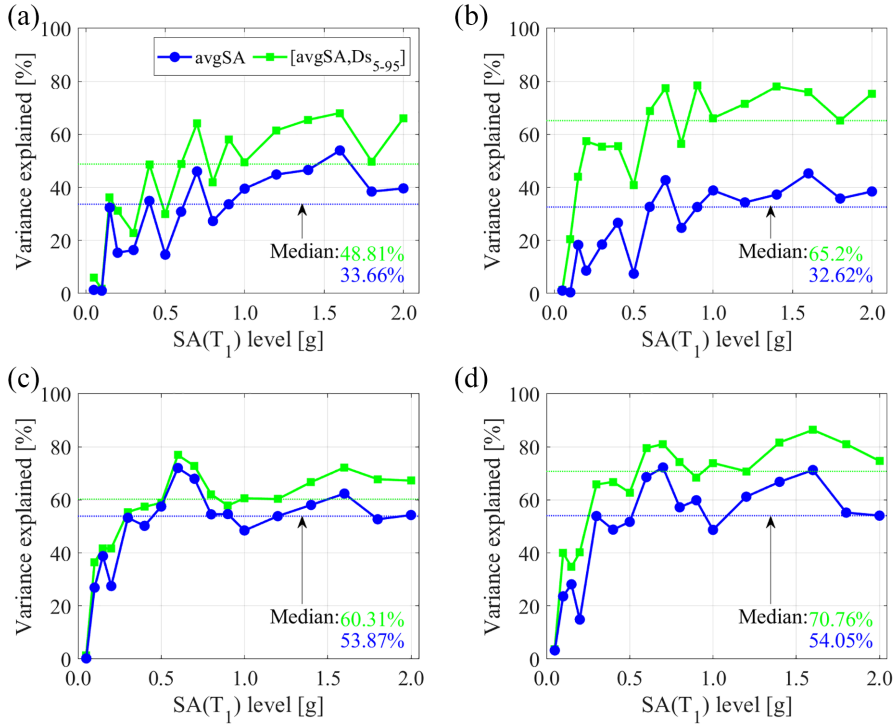
Figure 9. ANOVA for the case-study frames per $SA(T_1)$ level for (a) PI frame in terms of MIDR; (b) PI frame in terms of E_h; (c) SI frame in terms of MIDR; and (d) SI frame in terms of E_h.

or Belejo et al. (2017), for example. As a result, it is expected that the response variability is reduced when including duration-related IMs, and when including EDPs that are well correlated to duration. It is noted that the proportions of variance explained are marginally affected using one or another EDP for models conditioning on *avgSA*, with discrepancies of about 1.00% or less in median terms. When duration (i.e. Ds_{5-95}) is included in the models, E_h outperformed MIDR by being an efficient proxy to capture duration cumulative effects in the structural response. Notably, this agrees with the results introduced in Part I (among other previous studies; e.g. Belejo et al., 2017; Pan et al., 2020), which exhibited a high correlation between IM and structural response when cumulative-based EDPs are used, as opposed to peak-based ones. This can be intuitively inferred from the definition of E_h since it depends on (and reflects) the response of every structural component on a cumulative basis, whereas when using MIDR, the level of damage depends on a maximum/peak global response.

For the PI frame, the proportion of variance explained by *avgSA* is considerably lower compared with the variance explained by [*avgSA, Ds_{5-95}*]; in median terms, approximately 15.15% using MIDR and 32.58% using E_h. This confirms that a combination of amplitude- and duration-related IMs can better estimate the structural response of the considered frames. Such behavior is particularly apparent when using E_h because the cumulative damage process associated with long-duration ground motions is better represented by this EDP. It is worth noting that the response, in terms of both the considered EDPs, can be equally explained when conditioning on *avgSA* only, with a 1.04% difference in median terms. For the SI frame, the proportion of variance explained by *avgSA* is similar to the

variance explained by [*avgSA*, Ds_{5-95}]; in median terms, approximately 6.44% lower using MIDR and 16.71% lower using E_h. Again, the response, in terms of both the considered EDPs, can be equally explained when conditioning on *avgSA* only, with a 0.18% difference in median terms. Hence, it is clear that ground-motion duration can effectively impact the nonlinear structural performance of the considered case studies. The above results agree well with those described in Part I, where duration effects are especially significant for highly deteriorating structural systems (i.e. for the PI frame). Moreover, minor discrepancies at low-intensity levels are found in terms of MIDR since duration effects are apparent when a structure reaches its peak strength and starts to strain-soften using this EDP, as observed in Part I and past investigations (e.g. Chandramohan et al., 2016b). Nevertheless, significant discrepancies are found at low-intensity levels for E_h since duration effects are apparent immediately after the yielding strength for this EDP, agreeing with the findings made in Part I also. It is worth mentioning that for a *special-code* structure, the differences in the response variability are much lower (but still significant) than those exhibited for a *pre-code* structure when using peak- or cumulative-based EDPs. This is because several inelastic cycles can occur in highly ductile structural systems (i.e. SI frame), causing the steady ratcheting of drifts. Since the adopted hysteretic models present a twofold deterioration behavior based on E_h (i.e. causing both strength and stiffness deterioration), it is expected that MIDR approximates the E_h proportion of the variance explained under a gradual structural hysteric deterioration.

Vector-valued fragility models

The general trend observed when deriving vector-valued fragility and vulnerability models is their strong dependence on the selected EDP, confirming the ANOVA results. When expressing the fragility models in terms of MIDR, the ground-motion duration effects are apparent only at high *avgSA* levels. In contrast, for the fragility models in terms of E_h, the impact of duration can be noticed at lower *avgSA* levels. For the PI frame, duration effects are evident at a wide range of intensity levels, confirming that duration can be important in highly deteriorating structures, also strengthening the results in Part I of this study. Similar behavior is noticed for the SI frame, yet to a lesser degree (at high-intensity levels). In Figure 10a and b, a comparison of the DS4 fragility model is derived by expressing structural response in terms of MIDR and E_h is shown, specifically for the PI and SI frames. It is worth noting that the observed differences in fragility and vulnerability estimates are statistically significant. This is corroborated by hypothesis testing on the significance of the probabilistic seismic demand models' regression coefficients, assuming that those are equal to zero as the null hypothesis while being different from zero as the alternative hypothesis, with a 95% significance level (i.e. choosing an I-type risk, equal to 0.05). Given that the obtained *p*-values are smaller than the conventional threshold of 0.05, the outcomes are considered statistically significant (e.g. Neter et al., 1996). Those observations can be propagated to the vulnerability models since the total probability theorem is used.

When using the MIDR as an EDP, significant duration effects are expected only if the structural components undergo cyclic deterioration or strain-softening since they are only indirectly captured by the computational (i.e. numerical) model. For the PI frame, expressing the response in terms of MIDR yields larger fragility median values for any combination of *avgSA* and Ds_{5-95}, concerning the results in E_h terms (Figure 10a). Considerable probability of exceedance DS4 (and other DSs in general) is expected even for relatively short-duration ground motions (i.e. durations up to approximately $Ds_{5-95} = 25$ *s*) at *avgSA*
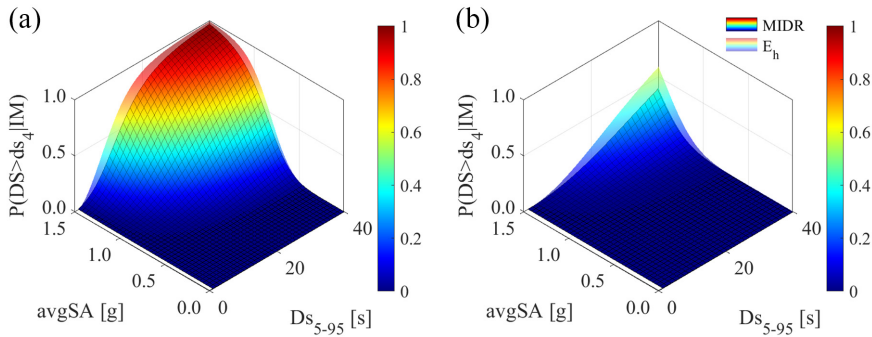
Figure 10. Comparison of DS4 fragility models in MIDR and E_h terms for (a) PI frame; (b) SI frame. The gridded opaque surfaces correspond to the models in terms of MIDR, and the non-gridded translucent surfaces correspond to the models in terms of E_h.

levels above ~0.50 g. This is expected, given the low ductility and energy dissipation capacity of this system, in turn, due to its poor structural detailing. Conversely, the SI frame's structural capacity is high enough not to cause structural collapse (unless reaching particularly high-intensity levels). Therefore, duration effects are negligible even at very high *avgSA* levels, up to ~1.00 g (Figure 10b). Nevertheless, a more apparent influence of duration is observed when using E_h at comparatively lower *avgSA* levels, although such effect is relatively small. It is important to stress that, conceptually, structures with higher energy dissipation capacity can be more affected by cumulative damage due to duration; however, at least for the SI frame, this occurs at unrealistic or infrequent intensity levels (both in terms of ground-motion amplitude and duration).

To better observe how the fragility varies with duration, fragility relationships conditioned on a scalar (i.e. *avgSA* only) and a vector-valued IM (i.e. $[Ds_{5-95}, avgSA]$) are compared for the PI frame for the two selected EDPs (Figure 11a and b). The scalar fragility relationship is derived using a similar approach as the one described in this study, but conditioning on *avgSA* only. The vector-valued fragility relationships are simply cuts of the fragility model shown in Figure 10a for arbitrarily selected Ds_{5-95} values. It is noted that duration exerts a critical influence even for DSs as low as DS1, but the fragility median values can be larger or smaller depending on the conditioning value of Ds_{5-95} as observed before. For instance, by expressing the structural response in MIDR terms, the DS4 vector-valued fragility median value is 39.54% lower—when conditioning on *avgSA* and $Ds_{5-95} = 35$ s—(38.02% larger—when conditioning on *avgSA* and $Ds_{5-95} = 5$ s) than the scalar fragility median value—when conditioning on *avgSA* only. When the fragility model is expressed in terms of E_h, the fragility grows faster with the *avgSA* and Ds_{5-95} levels, providing lower fragility median values in comparison with the MIDR-based models (Table 7), even for short-duration ground motions (e.g. $Ds_{5-95} = 20$ s). This confirms the results in Part I of this study; when using MIDR as EDP, the fragility relationships associated with DS3 and DS4 are greatly affected by ground-motion duration, while a minor/modest impact is registered for DS1 and DS2. However, when using E_h as an EDP, the fragility relationships for all the DSs are significantly impacted by duration, mainly for higher DSs when the structures approach their peak strength (or deformation).

Finally, Figure 12a and b shows a comparison between the E_h-based fragility models of the building frames in the infilled and bare configurations. It is worth mentioning that the
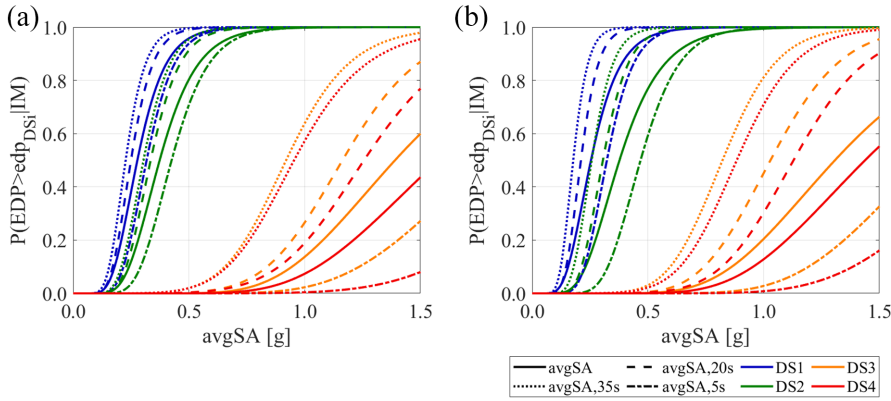
Figure 11. Fragility relationships conditioned on Ds_{5-95} values for the PI frame in terms of (a) MIDR; (b) E_h. The continuous fragility curves neglect duration.

Table 7. Fragility relationship parameters conditioning on *avgSA* and Ds_{5-95} values for the PI frame (relative difference estimated using $\mu_{avgSA\,|\,DS}$ in terms of MIDR as benchmark case per each DS)

DSs	EDPs	$\mu_{avgSA\,|\,DS}$	$\mu_{avgSA\,|\,DS,\,35s}$	$\mu_{avgSA\,|\,DS,\,20s}$	$\mu_{avgSA\,|\,DS,\,5s}$
DS1	MIDR	0.28	0.23	0.25	0.32
	Rel. diff. (%)	0.00	−18.05	−9.75	14.44
	E_h	0.25	0.18	0.21	0.28
	Rel. diff. (%)	−8.30	−36.10	−23.83	2.17
DS2	MIDR	0.37	0.30	0.33	0.42
	Rel. diff. (%)	0.00	−18.50	−10.19	13.94
	E_h	0.36	0.26	0.31	0.47
	Rel. diff. (%)	−4.29	−31.10	−17.96	25.47
DS3	MIDR	1.39	0.92	1.16	1.77
	Rel. diff. (%)	0.00	−33.81	−16.33	27.70
	E_h	1.31	0.82	1.03	1.69
	Rel. diff. (%)	−5.90	−40.86	−25.97	21.65
DS4	MIDR	1.58	0.95	1.26	2.18
	Rel. diff. (%)	0.00	−39.54	−20.41	38.02
	E_h	1.44	0.88	1.13	1.94
	Rel. diff. (%)	−8.87	−43.98	−28.45	23.00

PI: *pre-code* infilled; MIDR: maximum inter-story drift ratio; DS: damage state; EDP: engineering demand parameter.

masonry infills positively affect the fragility (higher fragility median values) both for the *pre-code* and the *special-code* frames. Although this is expected for the modern SI frame, such a positive effect of the infills for the bare frame indicates the absence of local effects (e.g. triggering of column shear failures) for the PI frame. In terms of duration, it is clear that duration impact is more apparent in the bare frames than in the infilled counterparts since their structural response is comparatively more influenced at low-to-moderate *avgSA* levels. Specifically, for the PB frame, it is noticed that duration effects can be neglected for an intensity level above ~0.50 g since a complete probability of exceedance DS4 (i.e. probability of exceedance DS4 equal to one) is achieved.
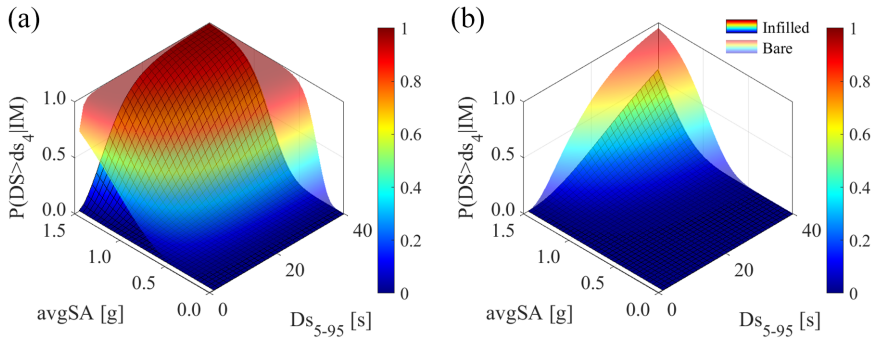
Figure 12. Comparison of DS4 fragility models in E_h terms for (a) PI frame versus PB frame; (b) SI frame versus SB frame. The gridded opaque surfaces correspond to the models for infilled frames, and the non-gridded translucent surfaces over the previous correspond to the models for bare frames.
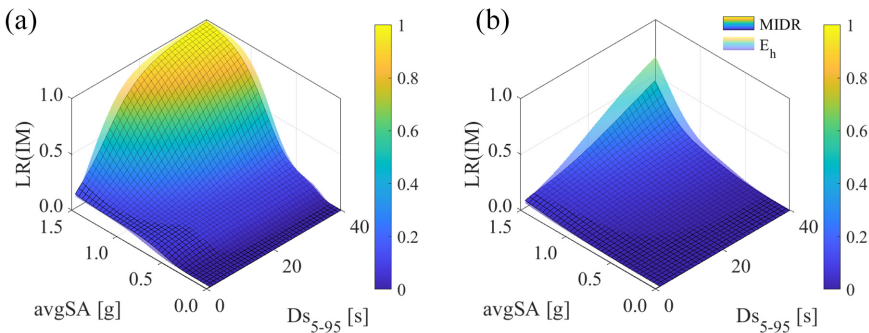
Figure 13. Comparison of vulnerability models in MIDR and E_h terms for (a) PI frame; (b) SI frame. The gridded opaque surfaces correspond to the models in terms of MIDR, and the non-gridded translucent surfaces over the previous correspond to the models in terms of E_h.

Vector-valued vulnerability models

As highlighted by the comparisons above in terms of fragility models, the LR is also strongly influenced by duration. Observing the vulnerability models for the PI (Figure 13a) and SI frame (Figure 13b), it is clear that accounting for duration explicitly (i.e. using E_h) provides a more insightful representation of the structural vulnerability as direct propagation from fragility results. For both case studies, for long (short) ground motions, the LR is generally higher (lower) than the results obtained neglecting duration effects (Table 8). If MIDR is used to assess the impact of duration on modern buildings as the SI frame, the differences in the LR can be considered negligible for an *avgSA* level below ~1.00 g, while using E_h can yield substantial differences in the LR, noticing a significant impact for an *avgSA* level from about ~0.80 g. It is worth mentioning again that the effect of ground-motion duration is more apparent for the PI frame since its peak strength can be achieved for moderate intensity levels, as opposed to the SI frame for the analyzed scenario.

To better understand the impact of ground-motion duration on vulnerability, a plot of the vulnerability relationships is developed using a scalar (i.e. *avgSA* only), and a vector-

Table 8. Vulnerability relationship values conditioning on *avgSA* and Ds_{5-95} for the PI frame (relative difference estimated using LR_{avgSA} in terms of MIDR as benchmark case per each *avgSA* level)

| *avgSA* level (g)	EDPs	LR_{avgSA}	$LR_{avgSA, 35s}$	$LR_{avgSA, 20s}$	$LR_{avgSA, 5s}$
0.5	MIDR	0.08	0.11	0.09	0.07
	Rel. diff. (%)	0.00	39.02	15.85	−10.98
	E_h	0.08	0.12	0.10	0.06
	Rel. diff. (%)	2.44	50.00	21.95	−23.17
1.0	MIDR	0.19	0.64	0.30	0.11
	Rel. diff. (%)	0.00	230.77	56.41	−42.56
	E_h	0.25	0.78	0.44	0.12
	Rel. diff. (%)	27.69	302.05	125.64	−40.51
1.5	MIDR	0.57	0.97	0.84	0.26
	Rel. diff. (%)	0.00	71.38	48.06	−54.42
	E_h	0.65	0.99	0.94	0.32
	Rel. diff. (%)	14.31	75.62	65.37	−43.46

PI: *pre-code* infilled; MIDR: maximum inter-story drift ratio; EDP: engineering demand parameter.
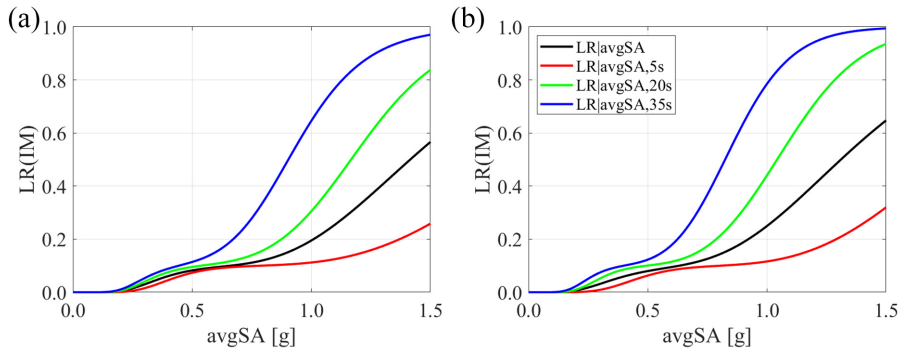
Figure 14. Vulnerability relationships conditioning on *avgSA* and Ds_{5-95} values for the PI frame in terms of (a) MIDR; (b) E_h. The black vulnerability curve neglects duration.

valued IM (i.e. $[Ds_{5-95}, avgSA]$) is shown in Figure 14a and b for comparison purposes (see LR values for different *avgSA* levels in Table 8). These vulnerability relationships are obtained through the total probability theorem using the fragility relationships described above (i.e. as outlined in the previous subsection) and a suitable damage-to-loss model. The discrepancies between the scalar and vector-valued vulnerability relationships are negligible—for engineering purposes—for low *avgSA* levels generally corresponding to an elastic response (see Figure 5 for the definition of the yielding points). The LR increases monotonically with Ds_{5-95}, leading to LR values that can be lower or higher than those predicted by a scalar vulnerability relationship, both in terms of MIDR or E_h (e.g. an LR 230.77% higher is attained when conditioning on both *avgSA* and $Ds_{5-95} = 35$ s rather than conditioning on *avgSA* only, by expressing structural response in MIDR terms).

Finally, masonry infills positively affect the structural vulnerability (reduce the LR for a given *avgSA* level). In Figure 15a and b, a comparison between vulnerability models of the building frames in infilled and bare configurations is shown. It is observed that the PB frame can achieve an LR = 1.00 for an *avgSA* level as low as ~0.50 g even at Ds_{5-95}
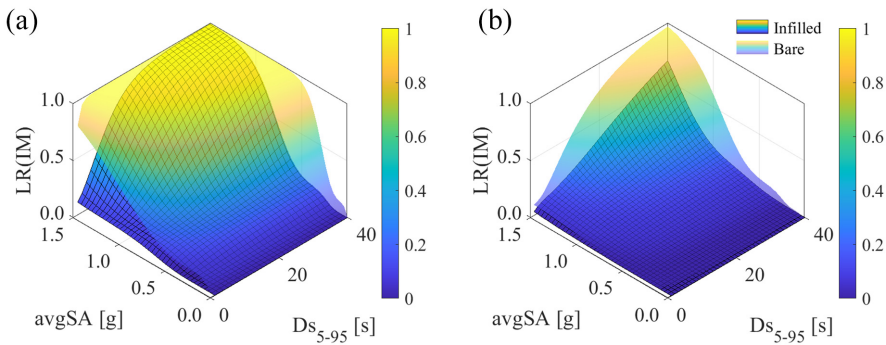
Figure 15. Comparison of vulnerability models in E_h terms for (a) PI frame versus PB frame and (b) SI frame versus SB frame. The gridded opaque surfaces correspond to the models for the infilled frames, and the non-gridded translucent surfaces over the previous correspond to the models for the bare frames.

moderate values, while the SB frame can achieve an LR > 0.70 for an *avgSA* level of ~1.00 g at high Ds_{5-95} values. The previous is directly propagated from fragility results. For the PB frame, duration impact can be neglected for *avgSA* levels above ~0.50 g since ground-motion amplitude fully controls the state of damage of this structure. For the other case-study frames, duration impact can be neglected for *avgSA* levels below ~0.50 g, given the low ground-motion amplitude. This result agrees with previous literature where duration effects are evident at high-intensity levels and vice versa, particularly for modern building structures.

Conclusions

This article describes an end-to-end seismic performance-based assessment framework to account for ground-motion duration effects in practical/realistic engineering applications, relying on site- and building-specific analyses. Specifically, two archetype RC moment-resisting building frames, representative of different seismic design levels, are selected and used in an infilled and a bare configuration (four case-study frames in total) to perform cloud-based NLTHAs. The analysis results are used (1) to assess ground-motion duration's impact on the structural response variability via ANOVA and (2) to derive vector-valued fragility and vulnerability models, accounting for spectral shape and duration.

The ANOVA allows estimating the contribution of ground-motion duration and spectral shape to the variability in the structural response. However, it is observed that the proportion of variance explained in the regression models conditioned on *avgSA* and Ds_{5-95} is higher using E_h rather than MIDR. However, it is noted that the differences in the proportion of variance explained in the regression models conditioned on *avgSA* (only) are negligible when using E_h or MIDR. Thus, E_h is considered much more efficient than MIDR by explicitly including duration as IM. Notably, duration effects on structural response are more apparent for highly deteriorating *pre*-code frames at moderate- to high-intensity levels.

The vector-valued fragility and vulnerability model results agreed with the findings made in Part I. In such regard, as duration increases, the probability of exceeding a DS for a given *avgSA* level also increases (i.e. lower fragility median values are obtained) and DSs less severe than collapse are impacted by ground-motion duration. Both the fragility and vulnerability models exhibit a monotonic trend when *avgSA* and Ds_{5-95} levels increase,

indicating that duration can actually impact damage/loss estimates, especially using E_h. Overall, it is confirmed that duration impact is more apparent at high *avgSA* levels than at low levels, agreeing also with previous literature (e.g. Chandramohan et al., 2016b).

In general, E_h can be considered a better structural performance indicator when dealing with structures prone to damage accumulation. It is worth mentioning that the derived fragility and vulnerability models in energy terms are based on converting deformation-based DS thresholds into energy-based ones; therefore, it retains the confidence of widely accepted and calibrated deformation-based DS thresholds. Although the results of this article show that E_h is a superior proxy for damage accumulation, relevant experimental data confirming the energy-based DS thresholds are needed to validate the energy-based fragility predictions.

Overall, ground-motion duration was found to provide a non-negligible impact on the nonlinear structural performance of the analyzed case-study frames. Hence, it is concluded that duration should be included in the current seismic performance-based and seismic risk assessment practice. This is better done by considering a hazard-consistent ground-motion record selection and defining the fragility (and thus vulnerability) modeling using vector-valued IMs (e.g. $[Ds_{5-95}, avgSA]$) and cumulative-based EDPs (e.g. E_h), explicitly capturing the damage accumulation of a particular structural system.

ORCID iDs

Kenneth Otárola ![iD] https://orcid.org/0000-0002-5425-4423
Roberto Gentile ![iD] https://orcid.org/0000-0002-7682-4490

References

Aljawhari K, Gentile R, Freddi F and Galasso C (2021) Effects of ground-motion sequences on fragility and vulnerability of case-study reinforced concrete frames. *Bulletin of Earthquake Engineering* 19: 6329–6359.

Ancheta TD, Darragh RB, Stewart JP, Seyhan E, Silva WJ, Chiou BSJ, Wooddell KE, Graves RW, Kottke AR, Boore DM, Kishida T and Donahue JL (2014) NGA-West2 database. *Earthquake Spectra* 30(3): 989–1005.

Baker JW (2007) Probabilistic structural response assessment using vector-valued intensity measures. *Earthquake Engineering and Structural Dynamics* 36(13): 1861–1883.

Baker JW and Cornell CA (2005) A vector-valued ground motion intensity measure consisting of spectral acceleration and epsilon. *Earthquake Engineering and Structural Dynamics* 34(10): 1193–1217.

Baker JW and Cornell CA (2006) Spectral shape, epsilon and record selection. *Earthquake Engineering and Structural Dynamics* 35(9): 1077–1095.

Barani S, Spallarossa D and Bazzurro P (2009) Disaggregation of probabilistic ground-motion Hazard in Italy. *Bulletin of the Seismological Society of America* 99(5): 2638–2661.

Barbosa AR, Ribeiro FLA and Neves LAC (2017) Influence of earthquake ground-motion duration on damage estimation: Application to steel moment resisting frames. *Earthquake Engineering and Structural Dynamics* 46(1): 27–49.

Belejo A, Barbosa AR and Bento R (2017) Influence of ground motion duration on damage index-based fragility assessment of a plan-asymmetric non-ductile reinforced concrete building. *Engineering Structures* 151: 682–703.

Belsley DA (1991) A guide to using the collinearity diagnostics. *Computer Science in Economics and Management* 4(1): 33–50.

Bojórquez E, Iervolino I, Reyes-Salazar A and Ruiz SE (2012) Comparing vector-valued intensity measures for fragility analysis of steel frames in the case of narrow-band ground motions. *Engineering Structures* 45: 472–480.

Boore DM and Thompson EM (2014) Path durations for use in the stochastic-method simulation of ground motions. *Bulletin of the Seismological Society of America* 104(5): 2541–2552.

Bradley BA (2010) A generalized conditional intensity measure approach and holistic ground-motion selection. *Earthquake Engineering and Structural Dynamics* 39(12): 1321–1342.

Bradley BA (2011) Correlation of significant duration with amplitude and cumulative intensity measures and its use in ground motion selection. *Journal of Earthquake Engineering* 15(6): 809–832.

Bradley BA (2012) A ground motion selection algorithm based on the generalized conditional intensity measure approach. *Soil Dynamics and Earthquake Engineering* 40: 48–61.

Bravo-Haro MA and Elghazouli AY (2018) Influence of earthquake duration on the response of steel moment frames. *Soil Dynamics and Earthquake Engineering* 115: 634–651.

Burton H and Deierlein G (2014) Simulation of seismic collapse in nonductile reinforced concrete frame buildings with masonry infills. *Journal of Structural Engineering* 140(8): 1–10.

Calvi GM, Magenes G and Pampanin S (2002a) Experimental test on a three storey RC frame designed for gravity only. In: *Proceedings of the twelfth European conference on earthquake engineering* (Paper reference 727), London, UK; 9–13 September 2002.

Calvi GM, Magenes G and Pampanin S (2002b) Relevance of beam-column joint damage and collapse in RC frame assessment. *Journal of Earthquake Engineering* 6(1): 75–100.

Chandramohan R, Baker JW and Deierlein GG (2016a) Impact of hazard-consistent ground motion duration in structural collapse risk assessment. *Earthquake Engineering and Structural Dynamics* 45(8): 1357–1379.

Chandramohan R, Baker JW and Deierlein GG (2016b) Quantifying the influence of ground motion duration on structural collapse capacity using spectrally equivalent records. *Earthquake Spectra* 32(2): 927–950.

Consiglio dei Ministri (1939) *Regio Decreto Legge n. 2229 del 16/11/1939* (G.U. n.92 del 18/04/1940). Gazzetta Ufficiale Italiana.

Di Pasquale G, Orsini G and Romeo RW (2005) New developments in seismic risk assessment in Italy. *Bulletin of Earthquake Engineering* 3(1): 101–128.

Dobry R, Idriss IM and Ng E (1978) Duration characteristics of horizontal components of strong-motion earthquake records. *Bulletin of the Seismological Society of America* 68(5): 1487–1520.

Douglas J (2021) *Ground Motion Prediction Equations 1964-2021*. Glasgow: University of Strathclyde. Available at: http://www.gmpe.org.uk/gmpereport2014.pdf (accessed 25 February 2022).

Du W, Yu X and Ning CL (2020) Influence of earthquake duration on structural collapse assessment using hazard-consistent ground motions for shallow crustal earthquakes. *Bulletin of Earthquake Engineering* 18(7): 3005–3023.

Eads L, Miranda E and Lignos DG (2015) Average spectral acceleration as an intensity measure for collapse risk assessment. *Earthquake Engineering and Structural Dynamics* 44(12): 2057–2073.

Elefante L, Jalayer F, Iervolino I and Manfredi G (2010) Disaggregation-based response weighting scheme for seismic risk assessment of structures. *Soil Dynamics and Earthquake Engineering* 30(12): 1513–1527.

Eurocode 8 (2005) *European Standard EN 1998–3:2005: Design of Structures for Earthquake Resistance—Part 3: Assessment and Retrofitting of Buildings*. Brussels: Comite Europeen de Normalisation.

Fisher RA (1992) *Statistical Methods for Research Workers*. DOI: 10.1007/978-1-4612-4380-9_6.

Forte G, Chioccarelli E, De Falco M, Cito P, Santo A and Iervolino I (2019) Seismic soil classification of Italy based on surface geology and shear-wave velocity measurements. *Soil Dynamics and Earthquake Engineering* 122: 79–93.

Gentile R and Galasso C (2021) Hysteretic energy-based state-dependent fragility for ground-motion sequences. *Earthquake Engineering & Structural Dynamics* 50(4): 1187–1203.

Haselton CB and Deierlein GG (2008) Assessing seismic collapse safety of modern reinforced concrete moment-frame buildings. *Civil Engineering* 137: 1–128.

Haselton CB, Liel AB, Taylor-Lange SC and Deierlein GG (2016) Calibration of model to simulate response of reinforced concrete beam-columns to collapse. *ACI Structural Journal* 113(6): 1141–1152.

Huang C and Galasso C (2019) Ground-motion intensity measure correlations observed in Italian strong-motion records. *Earthquake Engineering and Structural Dynamics* 48(15): 1634–1660.

Huang C, Tarbali K and Galasso C (2020) Correlation properties of integral ground-motion intensity measures from Italian strong-motion records. *Earthquake Engineering and Structural Dynamics* 49(15): 1581–1598.

Ibarra LF, Medina RA and Krawinkler H (2005) Hysteretic models that incorporate strength and stiffness deterioration. *Earthquake Engineering and Structural Dynamics* 34(12): 1489–1511.

Iervolino I, Chioccarelli E and Convertito V (2011) Engineering design earthquakes from multimodal hazard disaggregation. *Soil Dynamics and Earthquake Engineering* 31(9): 1212–1231.

Iervolino I, Giorgio M, Galasso C and Manfredi G (2010) Conditional hazard maps for secondary intensity measures. *Bulletin of the Seismological Society of America* 100(6): 3312–3319.

Iervolino I, Manfredi G and Cosenza E (2006) Ground motion duration effect on nonlinear seismic response. *Earthquake Engineering and Structural Dynamics* 35(1): 21–38.

Jalayer F and Cornell CA (2009) Alternative non-linear demand estimation methods for probability-based seismic assessments. *Earthquake Engineering and Structural Dynamics* 38(8): 951–972.

Jayaram N, Lin T and Baker JW (2011) A computationally efficient ground-motion selection algorithm for matching a target response spectrum mean and variance. *Earthquake Spectra* 27(3): 797–815.

Kass GV, Mood AM, Graybill FA and Boes DC (1974) Introduction to the theory of statistics, 3rd ed. *Journal of the American Statistical Association* 69(348): 1050–1051.

Kazantzi AK and Vamvatsikos D (2015) Intensity measure selection for vulnerability studies of building classes. *Earthquake Engineering and Structural Dynamics* 44(15): 2677–2694.

Kempton JJ and Stewart JP (2006) Prediction equations for significant duration of earthquake ground motions considering site and near-source effects. *Earthquake Spectra* 22(4): 985–1013.

Kohrangi M, Bazzurro P, Vamvatsikos D and Spillatura A (2017) Conditional spectrum-based ground motion record selection using average spectral acceleration. *Earthquake Engineering and Structural Dynamics* 46(10): 1667–1685.

Liberatore L and Decanini LD (2011) Effect of infills on the seismic response of high-rise RC buildings designed as bare according to Eurocode 8 [Infl uenza della tamponatura sulla risposta sismica di edifi ci in c.a. alti progettati come nudi con l'Eurocodice 8]. *Ingegneria Sismica* 28(3): 7–23.

Liberatore L and Mollaioli F (2015) Influence of masonry infill modelling on the seismic response of reinforced concrete frames. In: *Civil-comp proceedings*. DOI: 10.4203/ccp.108.87.

Lignos DG and Krawinkler H (2011) Deterioration modeling of steel components in support of collapse prediction of steel moment frames under earthquake loading. *Journal of Structural Engineering* 137(11): 1291–1302.

Luco N and Bazzurro P (2007) Does amplitude scaling of ground motion records result in biased nonlinear structural drift responses? *Earthquake Engineering and Structural Dynamics* 36(13): 1813–1835.

Luco N and Cornell CA (2007) Structure-specific scalar intensity measures for near-source and ordinary earthquake ground motions. *Earthquake Spectra* 23(2): 357–392.

Martins L and Silva V (2021) Development of a fragility and vulnerability model for global seismic risk analyses. *Bulletin of Earthquake Engineering* 19(15): 6719–6745.

Mazzoni S, McKenna F, Scott MH, Fenves GL. (2009) *Open system for earthquake engineering simulation user command-language manual, OpenSees version 2.0.* University of California, Berkeley.

Minas S and Galasso C (2019) Accounting for spectral shape in simplified fragility analysis of case-study reinforced concrete frames. *Soil Dynamics and Earthquake Engineering* 119: 91–103.

Mohammad Noh N, Liberatore L, Mollaioli F and Tesfamariam S (2017) Modelling of masonry infilled RC frames subjected to cyclic loads: state of the art review and modelling with OpenSees. *Engineering Structures* 150: 599–621.

Neter J, Kutner MH, Nachtsheim CJ and Wasserman W (1996) *Applied Linear Statistical Models.* Boston, MA: McGraw-Hill.

Otárola K, Gentile R, Sousa L and Galasso C (2023) *Impact of earthquake-induced ground-motion duration on nonlinear structural performance.* Part I: Spectrally equivalent records and inelastic single-degree-of-freedom systems. Earthquake Spectra (in press).

Page ES and Bellman R (1962) Adaptive control processes: A guided tour. *Journal of the Royal Statistical Society. Series A (General)* 125(1): 161–162.

Pampanin S, Calvi GM and Moratti M (2002) Seismic behaviour of RC beam-column joints designed for gravity loads. In: *12th European conference on earthquake engineering.* London, UK, 9–13 September 2002.

Pan Y, Ventura CE and Tannert T (2020) Damage index fragility assessment of low-rise light-frame wood buildings under long duration subduction earthquakes. *Structural Safety* 84: 101940.

Panagiotakos TB and Fardis MN (2001) Deformations of reinforced concrete members at yielding and ultimate. *ACI Structural Journal* 98(2): 135–148.

Quinde P, Terán-Gilmore A and Reinoso E (2021) Cumulative structural damage due to low cycle fatigue: An energy-based approximation. *Journal of Earthquake Engineering* 25(12): 2474–2494.

Rossetto T and Elnashai A (2003) Derivation of vulnerability functions for European-type RC structures based on observational data. *Engineering Structures* 25(10): 1241–1263.

Setzler EJ and Sezena H (2008) Model for the lateral behavior of reinforced concrete columns including shear deformations. *Earthquake Spectra* 24(2): 493–511.

Sezen H and Moehle JP (2004) Shear strength model for lightly reinforced concrete columns. *Journal of Structural Engineering* 130(11): 1696-1702.

Silva V, Crowley H, Pagani M, Monelli D and Pinho R (2014) Development of the OpenQuake engine, the Global Earthquake Model's open-source software for seismic risk assessment. *Natural Hazards* 72(3): 1409–1427.

Sousa L, Marques M, Silva V and Varum H (2017) Hazard disaggregation and record selection for fragility analysis and earthquake loss estimation. *Earthquake Spectra* 33(2): 529–549.

Stein S and Wysession M (2003) *An Introduction to Seismology, Earthquakes, and Earth Structure.* Oxford: Blackwell Publishing Ltd.

Trifunac MD and Brady AG (1978) A study on the duration of strong earthquake ground motion. *Bulletin of the Seismological Society of America* 65(3): 1–28.

Verderame GM, Ricci P, Esposito M, Sansiviero FC (2011) Le caratteristiche meccaniche degli acciai impiegati nelle strutture in c.a. realizzate dal 1950 AL 1980 (in Italian). In: *Associazione Italiana Calcestruzzo Armato e Precompresso (AICAP).*

Villar-Vega M, Silva V, Crowley H, Yepes C, Tarque N, Acevedo AB, Hube MA, Gustavo CD and María HS (2017) Development of a fragility model for the residential building stock in South America. *Earthquake Spectra* 33(2): 581–604.

Zareian F and Medina RA (2010) A practical method for proper modeling of structural damping in inelastic plane structural systems. *Computers and Structures* 88(1–2): 45–53.